ELSEVIER

Biophysical Chemistry 124 (2006) 81 – 89

Biophysical Chemistry

http://www.elsevier.com/locate/biophyschem

AFM imaging and theoretical modeling studies of sequence-dependent nucleosome positioning

Sabrina Pisano [a], Emanuela Pascucci [a], Stefano Cacchione [a], Pasquale De Santis [b], Maria Savino [a,c,*]

[a] *Dipartimento di Genetica e Biologia Molecolare, Università di Roma I "La Sapienza", P.le Aldo Moro 5, 00185 Rome, Italy*
[b] *Dipartimento di Chimica, Università di Roma I "La Sapienza", P.le Aldo Moro 5, 00185 Rome, Italy*
[c] *Istituto di Biologia e Patologia Molecolari del CNR, Italy*

Received 11 April 2006; received in revised form 11 May 2006; accepted 11 May 2006
Available online 7 July 2006

Abstract

Telomeric chromatin has different features with respect to bulk chromatin, since nucleosomal repeat along the chain is unusually short. We studied the role of telomeric DNA sequences on nucleosomal spacing in a model system. Nucleosomal arrays, assembled on a 1500-bp-long human telomeric DNA and on a DNA fragment containing 8 copies of the 601 strong nucleosome positioning sequence, have been studied at the single molecule level, by atomic force microscopy imaging. Random nucleosome positioning was found in the case of human telomeric DNA. On the contrary, nucleosome positioning on 601 DNA is characterized by preferential positions of nucleosome dyad axis each 200 bp. The AFM-derived nucleosome organization is in satisfactory agreement with that predicted by theoretical modeling, based on sequence-dependent DNA curvature and flexibility. The reported results show that DNA sequence has a main role, not only in mononucleosome thermodynamic stability, but also in the organization of nucleosomal arrays.

Keywords: Telomeres; Nucleosomal arrays; Atomic force microscopy; Theoretical modeling; DNA flexibility

1. Introduction

Telomeres are the specialized nucleoprotein structures that protect the ends of eukaryotic chromosomes [1,2]. Telomeric DNAs generally consist of short sequences (5–8 bp) repeated in tandem. In higher eukaryotes telomeres are organized in nucleosomal arrays, with an unusually short spacing [3]. In humans, the repeat length of telomeric nucleosomes is about 160 bp, 40 bp shorter than bulk chromatin [4].

We previously proposed that telomeric chromatin structural features are due mainly to the peculiarity of telomeric DNA sequences [5]. This hypothesis was thoroughly investigated at the mononucleosomal level. Since almost all telomeric repeated DNAs are out of phase with the 10-bp periodicity of B-DNA double helix, telomeric DNAs must be considered as the prototype of intrinsically straight DNA.

In principle, this DNA feature should give rise to higher free energy of nucleosome formation with respect to average genomic DNA. In the nucleosome, 147 bp of DNA wrap around the histone octamer, resulting in the strongest DNA curvature so far observed in DNA/protein complexes [6]. On the basis of these considerations, we calculated the free energy of telomeric nucleosome formation, applying the theoretical method developed by our research group, based on sequence-dependent DNA curvature and flexibility [7–9]. The theoretical prediction was found in very good agreement with measurements of the free energy of telomeric nucleosome formation, obtained by competitive reconstitution [10–12]. We found that telomeric nucleosomes are characterized by the highest free energy among all DNAs so far studied [5,11,12]. Moreover, by

* Corresponding author. Dipartimento di Genetica e Biologia Molecolare, Università di Roma I "La Sapienza", P.le Aldo Moro 5, 00185 Rome, Italy. Tel.: +39 6 49912238; fax: +39 6 4440812.
E-mail address: maria.savino@uniroma1.it (M. Savino).

0301-4622/$ - see front matter © 2006 Elsevier B.V. All rights reserved.
doi:10.1016/j.bpc.2006.05.012

footprinting analyses we showed that telomeric mononucleosomes occupy multiple positions, spaced each telomeric repeat [11,12].

Recently, in order to investigate a telomeric chromatin model system, we studied the organization of nucleosomal arrays formed on human telomeric sequences, at single molecule level, by atomic force microscopy (AFM) imaging [13].

We have compared nucleosomal organization on an 800-bp-long human telomeric DNA fragment (which can organize up to five nucleosomes) with that on a fragment of the same length containing four copies in tandem of the 5S-rDNA gene. This latter DNA was chosen on account of its well-known ability to organize stable nucleosomes [14,15], and has been previously shown to give rise to non-random behavior in subsaturated nucleosomal array populations analyzed by AFM [16].

In both cases the main features of nucleosomal organization were found in satisfactory agreement with those derived by a Monte Carlo approach, for nucleosomal arrays near to saturation (about four or five nucleosomes on each DNA molecule). Instead, for subsaturated nucleosomal arrays (two or three nucleosomes on each DNA molecule) the experimental and theoretical distributions were different, mainly in the case of telomeric nucleosomes. We interpreted the difference between experimental and theoretical nucleosomal organization, suggesting that the investigated systems were not perfectly equilibrated on mica and that the 2D distributions entrapped some nucleosome–nucleosome interactions present in solution (3D system) [13].

In this paper, we have studied nucleosomal arrays formed on a human telomeric DNA fragment longer (1500 bp) than that used in our previous study (800 bp) [13]. The increase in DNA length is essential to decrease the effect of the DNA ends on nucleosome positioning. Previous studies, by electrophoretic mobility shift assay, have suggested that the DNA ends influence nucleosome positioning, which depends on the nucleotide sequence and the DNA length [17]. In general, this phenomenon is assigned to entropic effects due to the induced constraints on the polynucleotide chain thermal mobility [18]. In cloned telomeric sequences, the ends contain non-telomeric DNA (restriction sequences), that enhances the preference for nucleosome end positioning.

As a reference sequence, we used a DNA construct containing 8 tandem 200-bp repeats of the 601 sequence. This DNA has a higher affinity for the histone octamer with respect to the 5S-rDNA and has a strong preference for a unique dyad axis position [19].

By AFM imaging, we found that nucleosome positioning on human telomeric DNA is random at all degrees of saturation. On the contrary, nucleosome positioning on 601 DNA multimers is deterministic, since nucleosomes are strongly positioned each 200 bp. In both cases, this feature is in satisfactory agreement with the prediction of the theoretical modeling, showing that sequence-dependent DNA mechanical properties are the main parameters in determining nucleosomal distribution.

2. Experimental

2.1. DNA fragments

The 601-200_8 DNA was prepared by digesting the plasmid pUC18/601-200_8 (a gift from D. Rhodes) with Xba I and *Eco*RI.

$^{5'}$AATTCGATACTC (GGGTTATGTGATGGACCCTA
TACGCGGCCGCCCTGGAGAATCCCGGTGCC
GAGGCCGCTCAATTGGTCGTAGCAAGCTCT
AGCACCGCTTAAACGCACGTACGCGCTGTC
CCCCGCGTTTTAACCGCCAAGGGGATTACT
CCCTAGTCTCCAGGCACGTGTCAGATATAT
ACATCCTGTGCATGTATTGAACAGCGACTC)$_8$
GGATATCTCTAG$^{3'}$

The H-Tel_{250} DNA was excised from the plasmid pTAG3 (a gift from M. Nakamura) by Aat II digestion and purified by gel extraction.

$^{5'}$ACGTCTAGATCCGAT (TTAGGG)$_{250}$
ATCGTCTTCGACGT$^{3'}$

The H-Tel_{135} was excised from the plasmid pSXneo (a gift from H. Cook) by Bam H1 and BglII double digestion and purified by gel extraction.

$^{5'}$GATCTGATATCATCGATGAATT (TTAGGG)$_{135}$
AATTGAGTCTCGGTACCCGGGATC$^{3'}$

The H-Tel_{28} was excised from the plasmid pUC19 by *Hin*dIII and *Eco*RI double digestion and purified by gel extraction.

$^{5'}$AGCTTGCATGCCTGCAGGTCGACTCTAGAGGATC-
CCCGG (TTAGGG)$_{28}$ TACCGAGCTCGA ATT$^{3'}$

The 223-bp *Crithidia* fragment was excised from the plasmid pPK 201/cat by BamHI digestion and purified by gel extraction.

$^{5'}$ GATCCCGCCTAAAATTCCAACCGAAAATCG
CGAGGTTACT
TTTTTGGAGCCCGAAAACCACCCAAAATCA
AGGAAAAATG
GCCAAAAAAATGCCAAAAAAATAGCGAAAATA
CCCCGAAAAT
TGGCAAAAATTAACAAAAAAATAGCGAATTT
CCCTGAATTT
TAGGCGAAAAAACCCCCGAAAATGGCCAAA
AACGCACTGA
AAATCAAAATCTGAACGTCTCGG $^{3'}$

2.2. Histone octamer preparation

H1–H5 stripped chromatin was prepared from chicken erythrocytes nuclei. Purified histone octamers were obtained from polynucleosomes by hydroxyapatite chromatography, as previously described [5].

2.3. Nucleosomal arrays reconstitution

Oligonucleosomes were reconstituted onto H-Tel_{250} and 601-200_8 by salt dilution at room temperature, using a 1:1 weight ratio of DNA to purified histone octamer. Samples at 1.0 M NaCl were incubated for 30 min at 25 °C and then diluted to 0.1 M NaCl by adding 10 mM Tris–HCl (pH 7.6) by five

dilution steps (at 20-min intervals). The final nucleosome concentration is about 20 mg/ml. All samples were fixed by dialysis with 0.1% glutaraldehyde in 10 mM Tris–HCl (pH 7.6); 1 mM EDTA for 3 h at 4 °C. Excess of glutaraldehyde was removed by a final dialysis for 16 h against 10 mM Tris–HCl (pH 7.6), 1 mM EDTA at 4 °C.

2.4. Sample preparation for AFM imaging

Immediately prior to loading the sample on mica surface, reconstituted oligonucleosomes were approximately diluted 10-fold on ice. 20 µl of the sample (DNA concentration 20 µg/ml) in 10 mM Tris–HCl (pH 7.6) and 1 mM EDTA was applied on spermidine-treated mica (SPD-mica), rinsed with deionized water after 3 min and dried with nitrogen.

In order to evaluate the possible influence of the support on internucleosomal center-to-center distances, images of canonical chicken erythrocyte chromatin loaded on the same surface were compared with those derived from AFM visualization on untreated mica [20].

Fig. 1 shows a typical image of H1–H5 stripped chicken erythrocytes chromatin (a) and the center-to-center internucleosomal distances frequency of a set of about 300 molecules (b). The mean internucleosomal distance is about 32 nm and

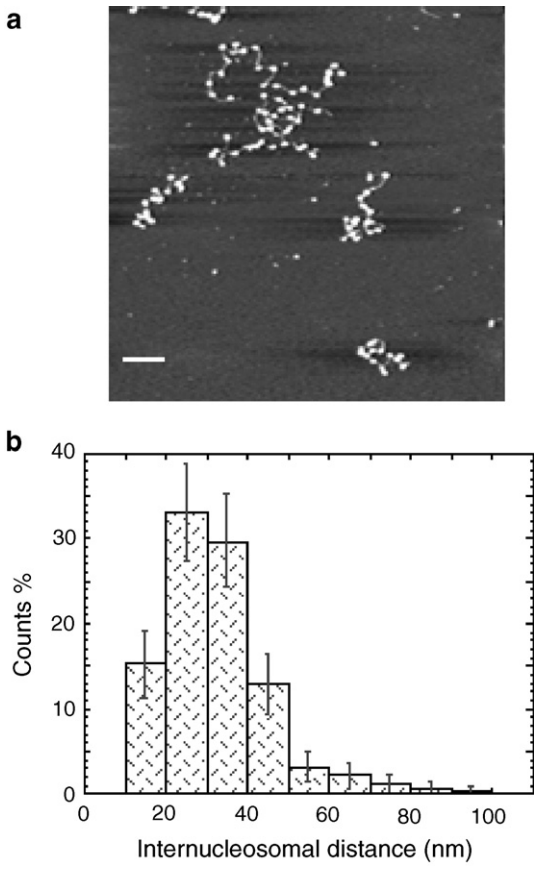

Fig. 1. Typical AFM image of H1–H5 stripped chromatin of chicken erythrocytes (a). Bar represents 100 nm. Relative histogram of internucleosomal distances (b). Errors on bin heights were evaluated as the square root of the number of counts.

corresponds quite satisfactorily to the value previously obtained by AFM images from chicken erythrocytes chromatin loaded on untreated mica [20]. This result has made us confident that in the adopted deposition time (3 min), the spermidine adsorbed on the mica surface does not influence internucleosomal distance frequency distributions.

2.5. AFM imaging

AFM images were taken with a MultiMode SPM instrument Nanoscope Digital III A, equipped with E-scanner (Digital Instruments Inc., Santa Barbara, CA), operating in tapping mode using canonical sharp silicon tips. AFM images of nucleosomal arrays were converted from Nanoscope format into TIF files and the internucleosomal (center-to-center) distance measurements were made using SigmaScan Pro software (SPSS Inc., Chicago, IL). Internucleosomal distances of molecules containing two, three, four, five, six, seven, and eight nucleosomes, respectively, were measured. For each class, about 60–200 molecules were examined in each of three independent experiments. Distance distributions were reported as histograms with bin size of 10 nm (about 26 bp), a value representative of AFM resolution power. To derive the length of the linker DNA from center-to-center internucleosomal distances, the nucleosome diameter was considered equal to 11 nm and the border-to-border internucleosomal distance was converted to base pairs considering 0.34 nm as the average distance of two nearest neighbor base pairs in B-DNA.

3. Results

3.1. Human telomeric DNA flexibility by AFM imaging

DNA flexibility measures the elastic property of the double helix axis to bend either in response of thermal stochastic perturbation by the environment or under a force field provided by the association with proteins. DNA flexibility depends on the sequence, since CG- or AT-rich sequences react differently.

Generally, the elastic property of DNA is represented by the persistence length (P), which measures the directional memory of the chain. P is related to b, the apparent elastic bending force constant, per base pair, according to the equation $P=0.34b/kT$. b is the bending stiffness of the chain, the inverse of the flexibility.

Different experimental techniques, such as circularization kinetics and dielectric rotational relaxation, permit to obtain the average flexibility of a DNA tract [21].

The statistical analysis of AFM images were also used to obtain the profile of flexibility along the sequence, when it is possible to determine the starting point of the sequence, from the standard deviation of the curvature [22].

Otherwise, it is possible to derive the average flexibility from the ratio between end-to-end distance and the contour length statistical ensemble of DNA images, only if the DNA tract does not contain intrinsic bends or curvature [23].

Telomeric DNAs are intrinsically straight, because of the sequence periodicity different from that of the double helix.

Therefore, DNA flexibility of telomeric sequences can be obtained by the simple evaluation of the average end-to-end distances and contour lengths, which is uniform along the DNA tract except at the terminals.

The Porod–Kratky formulation in 2D (1) permits to obtain the persistence length (P) which is strictly related to the flexibility [24].

$$\langle r^2 \rangle = 4PL_c[1-2P/L_c(1-e^{-L_c/2P})] \quad (1)$$

where $\langle r^2 \rangle$ is the end-to-end distance and L_c is the contour length.

We have studied the variations of end-to-end distances by increasing the length of human telomeric DNA molecules.

In Fig. 2, a gallery of typical AFM images of three telomeric DNAs of different length, H-Tel$_{35}$, H-Tel$_{135}$, H-Tel$_{250}$ is reported. In Fig. 2a, the shortest telomeric DNA, H-Tel$_{35}$, is visualized. It is worth noting that most molecules look as short sticks, since their length is near to the DNA persistence length. For the sake of comparison, we reported in Fig. 2b a typical AFM image of the strongly curved Crithidia fasciculata mithocondrial DNA fragment, approximately of the same length of H-Tel$_{35}$ (see Experimental). This feature is lost, increasing the telomeric DNA length (see Fig. 2c and d), since the ratio between the contour length and the end-to-end distance fits the Porod–Kratky equation. Thus, the values of the ratio between contour length and end-to-end distance as a function of the contour length of the three telomeric DNA fragments show that the persistence length of human telomeric DNA is equal to the persistence length of the average genomic DNA in solution, 50 nm, taking into account that our observations refer to 2D images on the mica surface (Fig. 3).

3.2. AFM imaging and internucleosomal distances distributions

AFM images were quantitatively characterized by measuring internucleosomal distances, since this parameter is directly connected to nucleosome positioning. Nucleosomal arrays formed onto H-Tel$_{250}$ and 601-200$_8$ were deposited on SPD-mica after glutaraldehyde fixation.

Fig. 4 shows typical AFM images of nucleosomal arrays reconstituted on H-Tel$_{250}$ (Fig. 4a), and on 601-200$_8$ (Fig. 4c); the distributions of the internucleosomal distances relative to the whole set of molecules, containing from two up to eight nucleosomes (Fig. 4b, d), are also reported.

The two internucleosomal distance distributions appear significantly different. While in the case of 601-200$_8$ DNA, a maximum is evident at about 35 nm, in the case of H-Tel$_{250}$, the frequency of internucleosomal distances monotonously

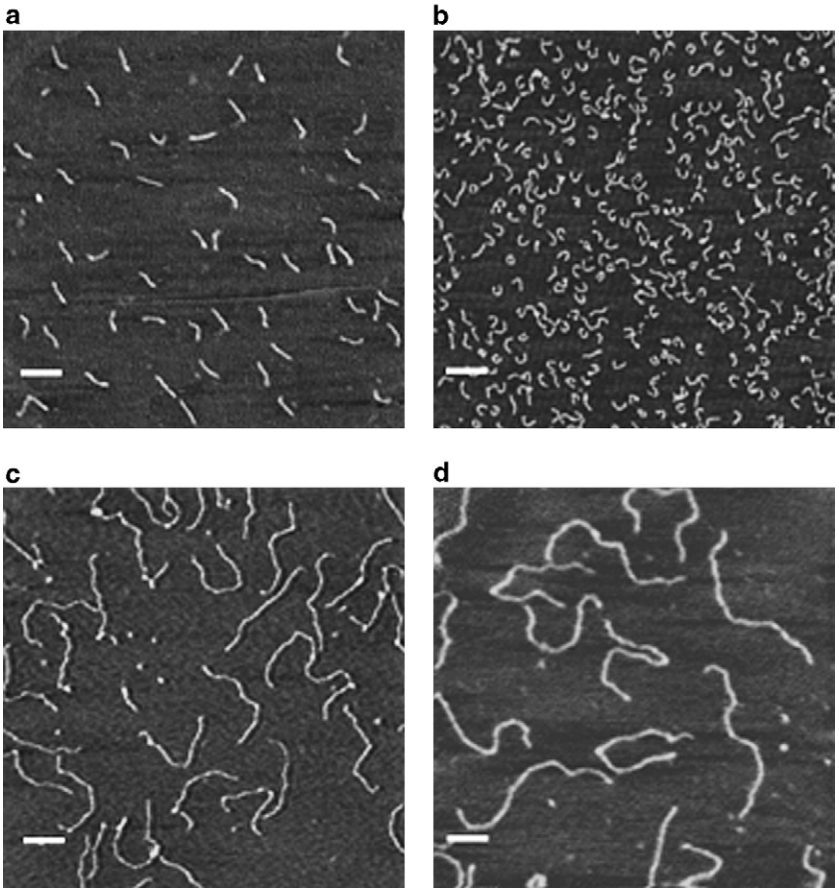

Fig. 2. Typical images of human telomeric DNA fragments, having the length of 220 bp (a), 800 bp (c), and 1500 bp (d). For the sake of comparison, a typical AFM image of the highly curved 223-bp-long mitochondrial DNA from C. fasciculata is also reported (b). Bar represents 100 nm.

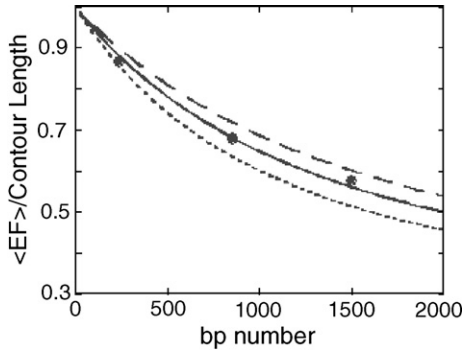

Fig. 3. Ratio between DNA contour length and end-to-end distance as a function of chain length, according to the Porod–Kratky model in a 2D system. The three curves correspond to three different persistence lengths: - – 60 nm, — 50 nm and - - - 40 nm, respectively. The filled circles represent the experimental values of the ratio $\langle ETE \rangle / L_c$, obtained by AFM imaging.

decreases. Since AFM allows to investigate nucleosomal arrays at single-molecule level, additional information can be obtained analyzing the internucleosomal distance distributions at various saturation levels. We divided the molecules visualized by AFM in groups, according to the number of nucleosomes in the arrays. In order to have a statistically significant number of molecules (at least 100 molecules), in some subsets, we have grouped molecules containing n and $n+1$ nucleosomes. It is worth recalling that eight nucleosomes should saturate the two DNAs. However, saturated DNA molecules often give rise to compact nucleosomal arrays (not shown) that have been eliminated from the counting.

In Fig. 5, the internucleosomal distance distribution of four different subsets are reported. The arrays containing two and three nucleosomes are grouped in the first subset (Fig. 5a, e); in Fig. 5b and f are reported molecules with four nucleosomes; in Fig. 5c and g are the molecules with five nucleosomes; in Fig. 5d and h are grouped arrays containing six, seven, and eight nucleosomes. Differences between the two DNAs are evident in all cases.

In all subsets, the internucleosomal distance distributions of H-Tel$_{250}$ DNA decrease monotonously. Increasing the nucleosome number, the internucleosomal distance distribution narrows, since the number of possible different internucleosomal distances decreases.

In Fig. 5d, the polynucleosomal organization is near to saturation and the most frequent internucleosomal distance is about 15 nm, corresponding to a distance between nucleosomes (linker DNA) of about 12 bp.

On the contrary, in the case of 601-200$_8$ DNA, the internucleosomal distance distributions (Fig. 5e–h) are characterized, in all groups, by a maximum centered at 35 nm (about 210 bp). In the subgroups containing from 2 to 5 nucleosomes, a second broader peak is evident (Fig. 5e–g), lower than the first one, at about 70 nm.

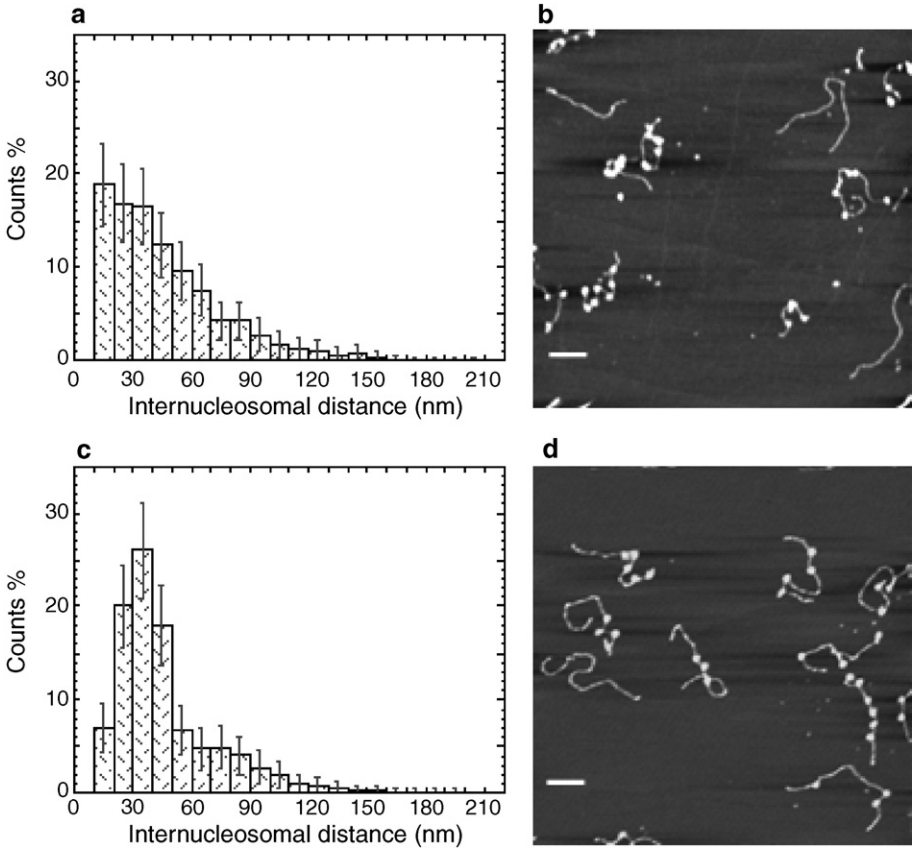

Fig. 4. Typical AFM images of nucleosomal arrays and the relative histograms of internucleosomal distances of H-Tel$_{250}$ (a, b) 601-200$_8$ (c, d). Error bars reflect the square root of the number of counts.

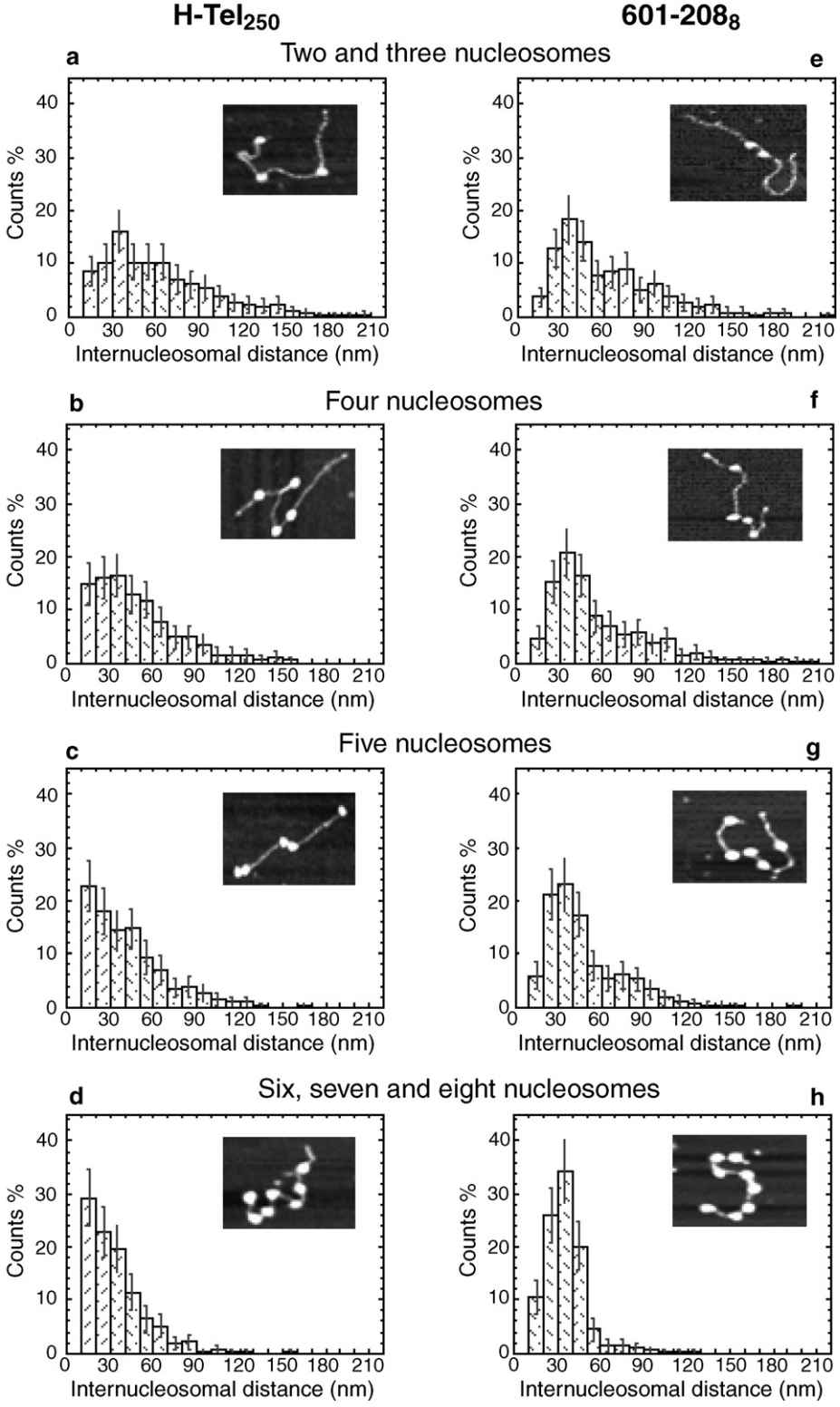

Fig. 5. Internucleosomal distance frequency distributions referring to H-Tel$_{250}$ (on the left) and 601-200$_8$ (on the right), respectively. Two and three nucleosomes (a, e); four nucleosomes (b, f); Five nucleosomes (c, g); six, seven and eight nucleosomes (d, h). In the inserts, typical polynucleosomal images are shown.

3.3. Theoretical modeling of nucleosomes positioning

We have developed a theoretical method, based on sequence-dependent DNA curvature and flexibility, which allows the quantitative prediction of the free energy of nucleosome formation in terms of thermodynamics and structural parameters of the dinucleotide steps [7,8]. If $\Delta G(k)$ represents the nucleosome reconstitution free energy difference of the kth DNA tract (defined as the nucleosome with its dyad at kth position of the sequence) with $L = 145$ bp along a sequence with

N bp, the free energy per mole of nucleosome, ΔG, pertinent to the whole DNA is

$$\beta\Delta G = -\ln \sum_{k=L/2}^{N-L/2} \exp[-\beta\Delta G(k)] \quad (2)$$

where β is $1/RT$. The exponential term represents the equilibrium constant pertinent to the nucleosome reconstitution of the kth DNA tract. The global reaction is considered as a sum of parallel reactions; for this reason, the different equilibrium constants, pertinent to all the possible nucleosome positions, sum up.

Using a statistical thermodynamic approach, we obtained $\Delta G(k)$ from the pertinent canonical partition functions. We evaluated the elastic contributions to the partition functions, related to the sum of the bending and twisting energies necessary to distort the intrinsic structure of the kth DNA tract in the nucleosomal form. Assuming first-order elasticity, we obtained [8]

$$\beta\Delta G_{el}(k) = \beta\Delta E^{\circ}_{el}(k) - 3/2(L\ln\langle T/T^{*}\rangle) + Z - Z\cos\varphi \quad (3)$$

where $\Delta E_{el}^{\circ}(k)$ is the minimum elastic energy required to distort the kth tract of L bp in the nucleosomal form; $\langle T/T^{*}\rangle$ is the average normalized dinucleotide empirical melting temperature of the kth DNA tract, which suitably represents the DNA differential rigidity, as supported by the analysis of DNA images by AFM [22]; Z is equal to $(\beta b/L)\langle T/T^{*}\rangle A_n A_f$. $A_n A_f$ represents the correlation between the curvature of the nucleosomal DNA and that of the free form in terms of the Fourier transform amplitudes of frequency 0.17 of the nucleosome and the free DNA curvature function along the L bp tract of the sequence, according to the convolution theorem, and φ is the angle between the directions of the effective intrinsic curvature and the nucleosome dyad axis.

The theoretical free energy values so obtained showed satisfactory agreement with the experimental data for a number of DNAs, but major deviations for others. This agreement, however, was strictly correlated ($R=0.99$) with the free DNA effective curvature, $\langle A_f\rangle$, which represents in modulus and phase the degree of similarity of the free DNA curvature with that of the nucleosome. This strongly indicated the existence of an additional curvature-dependent contribution to the free energy, which appears to destabilize the nucleosome. Such a contribution was obtained by fitting the free energy deviations by a simple function of the effective curvature [7,8]. We interpreted this free energy contribution as due to the groove contractions in intrinsically curved free DNAs, which stabilize the water spine and counterion interactions adding a further energy cost to the nucleosome formation. This contribution can be neglected for straight and slightly curved sequences.

If we calculate the free energy minima along a DNA sequence, long enough to accommodate more than one nucleosome, we can assume that the minima along the sequence represent virtual nucleosome positions.

Fig. 6 shows the nucleosome free energy profiles for H-Tel$_{250}$ and 601-200$_8$, respectively. The free energies of nucleosome formation are reported as a function of the nucleosome dyad position. The values of free energies are expressed relative to an intrinsically straight DNA with an average flexibility corresponding to a persistence length of 50 nm.

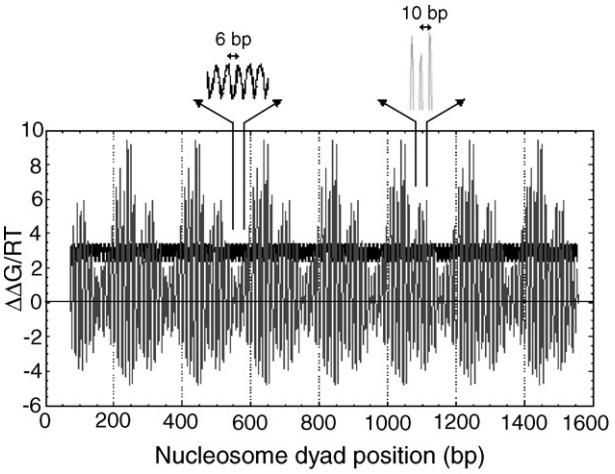

Fig. 6. Theoretical nucleosome dyad axis positioning on H-Tel$_{250}$ (black) and on 601-200$_8$ (grey). The free energy minima correspond to the energetically most favoured nucleosome dyad axis positions.

The profile referring to H-Tel$_{250}$ is characterized by multiple isoenergetic dyad axis positions, spaced every 6 bp (Fig. 6), in agreement with our previous experimental results at the mononucleosome level [10]. Since the free energy barrier is almost equal to thermal energy at room temperature, the probability of telomeric nucleosome positioning along DNA represents almost a continuum. On the contrary, the theoretical free energy profile of nucleosomal positioning, relative to 601-200$_8$ DNA, shows two minima, with 50 bp distance, for each monomer. The first position corresponds to the well-known nucleosome position on the Widom DNA fragment [19], while the second one derives from the multimerization in tandem of the sequence. The difference of the free energy of nucleosome formation between the two positions is not so high to give rise to a significant difference of nucleosome distributions. The distance of about 50 bp is likely to cause only the broadening of the histograms. Moreover, it must be taken into account that each minimum is embedded in a family of satellite minima, characterized by slightly higher free energy values, spaced each at 10 bp, and thus, rotationally phased with the B-DNA periodicity.

4. Discussion

In this paper, we compare nucleosomal organization on human telomeric DNA, derived from AFM imaging at single molecule level, with that predicted by the theoretical method we previously developed, based on sequence-dependent DNA curvature and flexibility [7,8]. Since telomeric DNA is straight, it was possible to derive its flexibility from AFM visualization. The obtained value of persistence length indicates average flexibility (Fig. 3), in agreement with our model that connects DNA flexibility to its nucleotide composition [7].

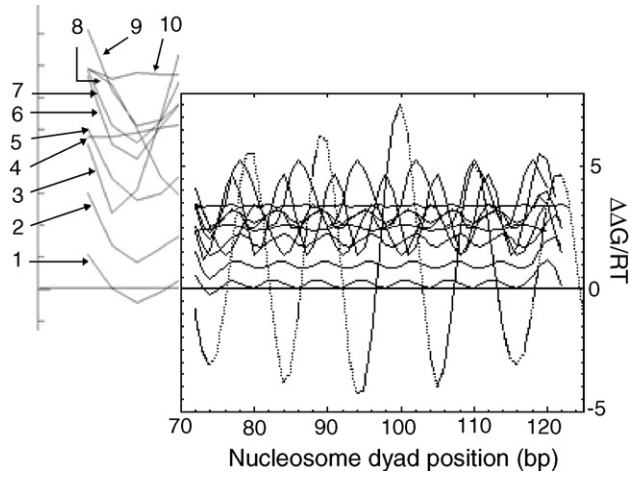

Fig. 7. Nucleosome positioning on telomeric DNAs. Each numbered arrow indicates the investigated telomeric sequence, reported in Table 1. Taking into account that all considered telomeric DNAs are repetitive, the length of the fragments has been made equal to 200 bp. For the sake of comparison, nucleosome positioning on a multimer in tandem of Widom 601 DNA, of the same length, has been reported.

Both experimental and theoretical analysis show that nucleosomes are randomly positioned on telomeric sequences. AFM visualizations of nucleosomal arrays at different degrees of saturation show a monotone decrease of frequency distributions, implying a random nucleosomal organization. (Fig. 4a, Fig. 5a–d). The theoretical analysis shows a multiple positioning of telomeric nucleosomes, with dyad axis positions spaced every 6 bp, the periodicity of human telomeric DNA (Fig. 6). Moreover, the barriers between adjacent free energy minima are so low that we can consider the nucleosomal organization on human telomeric DNA as almost continuous, and the nucleosome as freely moving along DNA. This feature should cause higher mobility of telomeric nucleosomes with respect to average nucleosomes. Preliminary results obtained in our laboratory by measuring the thermal mobility of telomeric nucleosomes seem consistent with this model (S. Pisano, E. Marchioni, A. Galati, M. Savino, S. Cacchione, unpublished results).

Interesting results emerge from the comparison of telomeric polynucleosomal organization with nucleosome positioning on 601-200_8 DNA. Since, at the moment, this DNA is the strongest known nucleosome positioning sequence [19], it represents the best available standard to test our chromatin model system based on DNA sequence-dependent polynucleosomal organization. As shown in Fig. 6, nucleosome positioning on 601-200_8 DNA is characterized by the repetition of two minima, each belonging to a family of rotationally phased satellite positions, characterized by slightly different free energy values.

The theoretically predicted internucleosomal distance along 601-200_8 DNA is 200 bp in the case of nucleosomes which occupy next neighbor minima, and of 400 bp in the case of nucleosomes which occupy alternate minima. This positioning correlates satisfactorily with the internucleosomal distance frequency distributions derived from AFM imaging, which are characterized by a maximum at about 35 nm (210 bp) and a lower and broader maximum at about 70 nm that disappears increasing the nucleosome number in the array (see Fig. 5 e–h).

The satisfactory agreement between experimental evaluation and theoretical prediction suggests that the nucleosomal organization depends mainly on sequence-dependent DNA mechanical features, at least in a system containing only histone octamer and DNA. It is worth remembering that the organization of nucleosomal arrays in vivo is modulated also by other constraints (i.e., regulative protein specific interactions).

On the basis of the obtained results, it seems interesting to predict the nucleosomal organization of telomeric DNAs from different eukaryotic systems. In Fig. 7, the predicted positioning of nucleosomes formed on various telomeric sequences with a repeat length between 5 and 8 bp is reported (Table 1), compared with that on the 601 DNA monomer. The main features of nucleosome positioning are similar among telomeric sequences and are dramatically different from those of 601 DNA. In the latter case, the energy minima are much lower than the average genomic DNA and are spaced every 10 bp, in phase with the B-DNA helical repeat. Moreover, the energy barrier between two consecutive minima is noticeably high. On the contrary, in telomeric sequences, the free energy minima of nucleosome formation are significantly high with respect to average genomic DNA. Besides, minima are spaced every telomeric repeat, out of phase with the double helix periodicity. The energy barrier that separates adjacent minima shows a broad variation among the different telomeric sequences. However, in all cases, the energy barrier is so small that at physiological temperature (37 °C), it is likely that nucleosomal distributions on telomeres of different species are similar.

Finally, our results suggest that AFM imaging seems an adequate method to study polynucleosomal systems at single molecule level [25].

Table 1
Telomeric DNA Sequences

Sequences	Species
[8]TTTTGGGG	*Euplotes*
	Oxytricha
	Stylonychia
[4]TTTTAGGG	*Chlamydomonas reinhardtii*
[3]TTTAGGG	*Arabidopsis thaliana*
	Plasmodium
	Tomato
[5]TTTGGG	*Paramecium*
[6]TTGGGG	*Glaucoma*
	Tetrahymena
[9]TTAGGGGG	*Cryptococcus neoformans*
[7]TTAGGG	*Didymium iridis*
	Fusarium oxysporum
	Human
	Mice
	Neurospora crassa
	Physarum polycephalum
	Podospora anserina
	Trypanosoma brucei
[1]TTAGGC	*Ascaris lumbricoides*
[2]TTACAG	*Schizosaccharomyces pombe*
[10]TAGGG	*Giardia lamblia*

Superscripted numbers refer to the theoretical analyses of nucleosome positioning reported in Fig. 7.

Acknowledgements

Thanks are due to R. Mechelli for AFM visualization of H1–H5 stripped chicken erythrocyte chromatin. This research has been financially supported by COFIN 2005 and by Istituto Pasteur–Fondazione Cenci Bolognetti.

References

[1] D. Kipling, The Telomere, Oxford University Press, 1995.
[2] D. Rhodes, L. Fairall, T. Simonsson, R. Court, L. Chapman, Telomere architecture, EMBO Rep. 3 (2002) 1139–1145.
[3] V.L. Makarov, S. Lejnine, J. Bedoyan, J.P. Langmore, Nucleosomal organization of telomere-specific chromatin in rat, Cell 73 (1993) 775–787.
[4] J.K. Bedoyan, S. Lejnine, V.L. Makarov, J.P. Langmore, Condensation of rat telomere-specific nucleosomal arrays containing unusually short DNA repeats and histone H1, J. Biol. Chem. 271 (1996) 18485–18493.
[5] S. Cacchione, M.A. Cerone, M. Savino, In vitro low propensity to form nucleosomes of four telomeric sequences, FEBS Lett. 400 (1997) 37–41.
[6] K. Luger, A.W. Mader, R.K. Richmond, D.F. Sargent, T.J. Richmond, Crystal structure of the nucleosome core particle at 2.8 Å resolution, Nature 389 (1997) 251–260.
[7] C. Anselmi, G. Bocchinfuso, P. De Santis, M. Savino, A. Scipioni, Dual role of DNA intrinsic curvature and flexibility in determining nucleosome stability, J. Mol. Biol. 286 (1999) 1293–1301.
[8] C. Anselmi, G. Bocchinfuso, P. De Santis, M. Savino, A. Scipioni, A theoretical model for the prediction of sequence-dependent nucleosome thermodynamic stability, Biophys. J. 79 (2000) 601–613.
[9] A. Scipioni, S. Pisano, C. Anselmi, M. Savino, P. De Santis, Dual role of sequence-dependent DNA curvature in nucleosome stability: the critical test of highly bent *Crithidia fasciculata* DNA tract, Biophys. Chemist. 107 (2004) 7–17.
[10] T.E. Shrader, D.M. Crothers, Effects of DNA sequence and histone–histone interactions on nucleosome placement, J. Mol. Biol. 216 (1990) 69–84.
[11] I. Filesi, S. Cacchione, P. De Santis, L. Rossetti, M. Savino, The main role of the sequence-dependent DNA elasticity in determining the free energy of nucleosome formation on telomeric DNAs, Biophys. Chemist. 83 (2000) 223–237.
[12] L. Rossetti, S. Cacchione, M. Fua, M. Savino, Nucleosome assembly on telomeric sequences, Biochemistry 37 (1998) 6727–6737.
[13] R. Mechelli, C. Anselmi, S. Cacchione, P. De Santis, M. Savino, Organization of telomeric nucleosomes: atomic force microscopy imaging and theoretical modeling, FEBS Lett. 566 (2004) 131–135.
[14] F. Dong, J.C. Hansen, K.E. van Holde, DNA and protein determinants of nucleosome positioning on sea urchin 5S rRNA gene sequences in vitro, Proc. Natl. Acad. Sci. U. S. A. 87 (1990) 5724–5728.
[15] G. Meersseman, S. Pennings, E.M. Bradbury, Chromatosome positioning on assembled long chromatin. Linker histones affect nucleosome placement on 5 S rDNA, J. Mol. Biol. 220 (1991) 89–100.
[16] J.G. Yodh, Y.L. Lyubchenko, L.S. Shlyakhtenko, N. Woodbury, D. Lohr, Evidence for nonrandom behavior in 208-12 subsaturated nucleosomal array populations analyzed by AFM, Biochemistry 38 (1999) 15756–15763.
[17] G. Meersseman, S. Pennings, E.M. Bradbury, Mobile nucleosomes: a general behavior, EMBO J. 11 (1992) 2951–2959.
[18] T. Sakaue, K. Yoshikawa, S.H. Yoshimura, K Takeyasu, Histone core slips along DNA and prefers positioning at the chain end, Phys. Rev. Lett. 87 (2001) 078105-1/078105-5.
[19] P.T. Lowary, J. Widom, New DNA sequence rules for high affinity binding to histone octamer and sequence-directed nucleosome positioning, J. Mol. Biol. 276 (1998) 19–42.
[20] S.H. Leuba, C. Bustamante, K. van Holde, J. Zlatanova, Linker histone tails and N-tails of histone H3 are redundant: scanning force microscopy studies of reconstituted fibers, Biophys. J. 74 (1998) 2830–2839.
[21] C. Anselmi, G. Bocchinfuso, P. De Santis, M. Savino, A. Scipioni, Statistical thermodynamic approach for evaluating the writhe transformations in circular DNA, J. Phys. Chem. 102 (1998) 5704–5714.
[22] G. Zuccheri, A. Scipioni, V. Cavaliere, G. Gargiulo, P. De Santis, B. Samori, Mapping the intrinsic curvature and flexibility along the DNA chain, Proc. Natl. Acad. Sci. U. S. A. 98 (2001) 3074–3079.
[23] C. Rivetti, C. Walker, C. Bustamante, Polymer chain statistics and conformational analysis of DNA molecules with bends or sections of different flexibility, J. Mol. Biol. 280 (1998) 41–59.
[24] C.R. Cantor, P.R. Schimmel, Biophysical Chemistry Part III: The Behavior of Biological Macromolecules, W.H. Freeman and Company, 1980.
[25] H.G. Hansma, K. Kasuya, E. Oroudjev, Atomic force microscopy imaging and pulling of nucleic acids, Curr. Opin. Struct. Biol. 14 (2004) 380–385.